ARTICLES

Cells keep a memory of their tissue origin during axolotl limb regeneration

Martin Kragl[1,3]*†, Dunja Knapp[1,3]*, Eugen Nacu[1,3], Shahryar Khattak[1,3], Malcolm Maden[4], Hans Henning Epperlein[2] & Elly M. Tanaka[1,3]

During limb regeneration adult tissue is converted into a zone of undifferentiated progenitors called the blastema that reforms the diverse tissues of the limb. Previous experiments have led to wide acceptance that limb tissues dedifferentiate to form pluripotent cells. Here we have reexamined this question using an integrated GFP transgene to track the major limb tissues during limb regeneration in the salamander *Ambystoma mexicanum* (the axolotl). Surprisingly, we find that each tissue produces progenitor cells with restricted potential. Therefore, the blastema is a heterogeneous collection of restricted progenitor cells. On the basis of these findings, we further demonstrate that positional identity is a cell-type-specific property of blastema cells, in which cartilage-derived blastema cells harbour positional identity but Schwann-derived cells do not. Our results show that the complex phenomenon of limb regeneration can be achieved without complete dedifferentiation to a pluripotent state, a conclusion with important implications for regenerative medicine.

The salamander is a powerful regeneration model because it can reconstitute a fully functional limb after injury. Amputation anywhere between the shoulder and the hand triggers the formation of a progenitor cell zone called the blastema that regenerates the missing portion. The mature limb consists of multiple tissues, including the epidermis, dermis, muscle, nerve, blood vessels and skeletal elements that potentially contribute to the blastema, and these tissues must regenerate coordinately to restore functionality. In addition, the limb is structured into three major segments—upper arm, lower arm and hand, generically termed the proximo-distal axis—that must be properly patterned. Remarkably, the fundamental questions of which tissues contribute to the blastema, and whether blastema cells are a multipotent or pluripotent cell type have remained largely unanswered, owing to the complexity of the adult limb as an experimental starting point and the lack of tools with which to follow different cell types precisely over the course of regeneration.

Histologically, the blastema appears to be a homogeneous group of cells and has been commonly viewed as a single cell type. Considering that multiple tissue types in the limb are regenerated, this would imply that blastema cells are pluripotent. Indeed, many studies have suggested that cells become multipotent or pluripotent in the limb blastema[1]. When the bones were removed from salamander limbs before amputation, the resulting regenerates contained all limb tissues including the bone, implying that non-skeletal cells converted to bone during regeneration, and skin was identified as one potential source of skeleton[2–6].

Muscle and Schwann cells have also been proposed to achieve a multipotent or pluripotent state during limb regeneration. Wallace and Wallace observed full limb regeneration after implanting nerve pieces into irradiated hosts and hypothesized that Schwann cells become pluripotent[7]. Muscle was also thought to acquire broad plasticity (for review see ref. 8). Experiments tracking dextran-injected newt myotubes implanted into the limb blastema found the label in cartilage, implying dedifferentiation of muscle into a multipotent progenitor[9]. Complementarily, BrdU was used to track cultured newt muscle satellite cells *in vivo*, where labelled cells populated cartilage, muscle and even epidermis[10]. Such apparent plasticity could, however, have been acquired during culturing, through BrdU incorporation into DNA or through label transfer to the host[11]. These experiments pointed out the need to mark the different limb cell types indelibly with high resolution, specificity and minimal perturbation.

Here, by comprehensively tracking limb tissues marked by an integrated green fluorescent protein (GFP)–transgene in the salamander *Ambystoma mexicanum* (the axolotl), we show that cells do not become pluripotent during limb regeneration and retain a strong memory of their tissue or embryonic origin. This leads to the important conclusion that the blastema is a heterogeneous pool of restricted progenitor cells from its outset. Using this information, we further show that proximo-distal positional identity is a tissue-specific property of blastema cells: blastema cells deriving from cartilage harbour positional identity but Schwann cells do not. This means that tissue-specific origin must be considered when studying any aspect of the limb blastema.

Dermis makes cartilage but not muscle or Schwann cells

We achieved specific labelling of each major limb tissue either by grafting the embryonic region that produces that limb tissue from GFP^+ transgenic donors[12] into GFP^- host embryos[13] or by direct grafting of a given GFP^+ limb tissue to an unlabelled host (see Figs 1, 2, 3, 4, Supplementary Fig. 3 and the online-only Methods). To draw our conclusions we examined thousands of cells in multiple individuals (quantification in Supplementary Tables). An important requirement of the donors is stable GFP–transgene expression. No chimaeric expression in the regenerate to indicate silencing was observed (Supplementary Fig. 2 and Supplementary Table 1).

Immediately after amputation, a layer of epidermal cells migrates over the stump and has long been considered to remain separate from the internal blastema[4,14]. Grafting of embryonic GFP^+ epidermis to label limb epidermis confirmed these results (Supplementary Fig. 3).

[1]Max Planck Institute of Molecular Cell Biology and Genetics, Pfotenhauerstrasse 108, [2]Institute of Anatomy, Medical Faculty, University of Technology Dresden, Fetscherstrasse 74, [3]Center for Regenerative Therapies, University of Technology Dresden, Tatzberg 47/49, 01307 Dresden, Germany. [4]The Regeneration Project, McKnight Brian Institute, University of Florida, Rm 326 Bartram Hall, Gainesville, Florida 32611, USA. †Present address: Institute of Metabolic Physiology, Heinrich-Heine-Universität Düsseldorf, Universitätsstrasse 1, 40225 Düsseldorf, Germany.
*These authors contributed equally to this work.

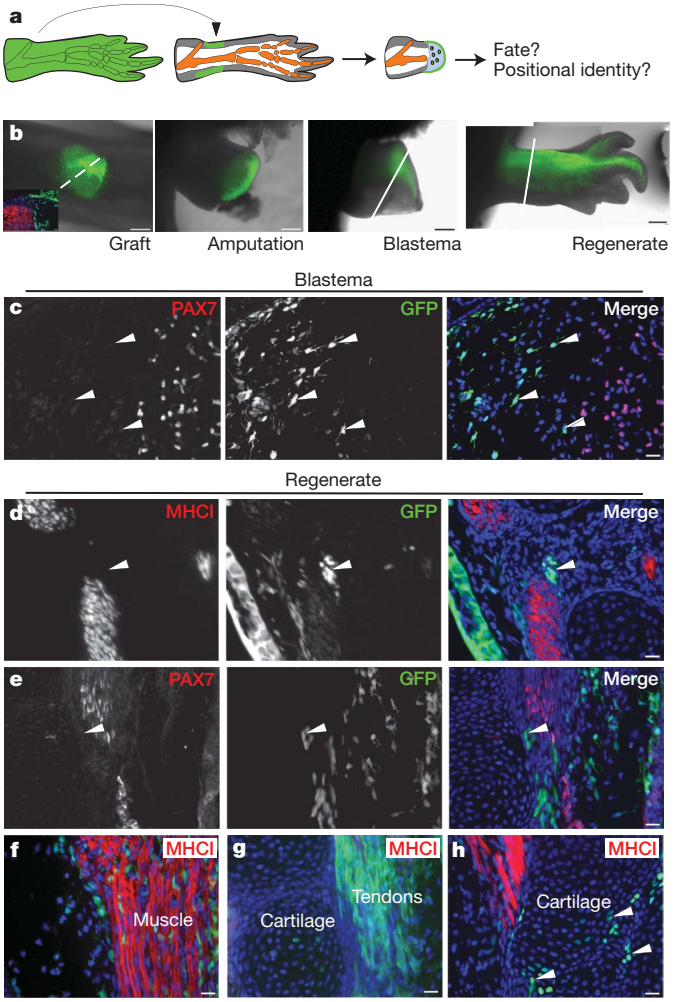

Figure 1 | Dermis does not make muscle but makes cartilage and tendons. **a**, Schematic of experiment. **b**, Representative time course. Inset shows cross-section at dashed line immunostained for MHCI (see Supplementary Fig. 4a, b). **c**, Longitudinal section of 12-day blastema. GFP^+ (arrowhead) and $PAX7^+$ signals did not overlap. **d**, **e**, Cross-sections through regenerated limbs. GFP^+ cells (arrowheads) were negative for the indicated muscle markers (red). **f**–**h**, Longitudinal sections immunostained for anti-MHCI. Fluorescent cells contributed to connective tissue (**f**), tendons (**g**) and cartilage (**h**, arrowheads). Blue shows DAPI in merge panels (**d**–**h**). Scale bars: **b**, 0.5 mm; **c**–**h**, 50 μm.

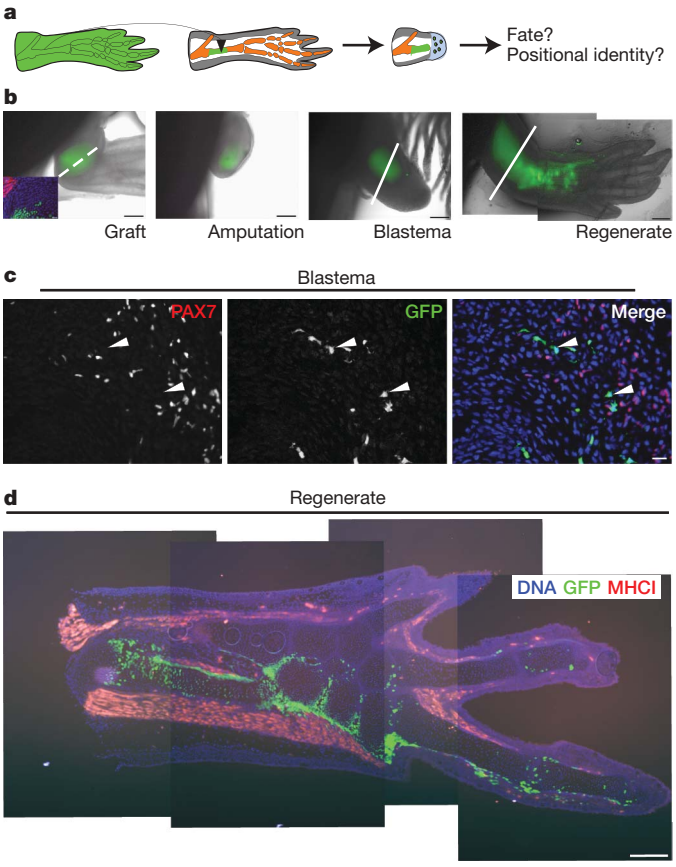

Figure 2 | Cartilage cells do not make muscle. **a**, Schematic of experiment. **b**, Time course through regeneration. Inset shows cross-section at dashed line immunostained for MHCI (see Supplementary Fig. 4c, d). **c**, Longitudinal section of a 12-day blastema. GFP^+ cells (arrowheads) were negative for $PAX7^+$ signals. **d**, Longitudinal section of a regenerated limb 30 days post-amputation immunostained for MHCI (red). The majority of fluorescent cells were found located in the regenerated skeleton; no signal was found in muscle. Blue shows DAPI in merge panels (**b**–**d**). Scale bars: **b**, 0.5 mm; **c**, 50 μm; **d**, 100 μm.

In contrast, the dermal layer of skin is a major contributor to the blastema, and has been proposed to have potent patterning effects on regeneration[15–19]. To determine whether dermis produces a pluripotent cell, we grafted full-thickness skin from GFP^+ transgenic 8-cm-long donors onto GFP^- hosts (Fig. 1a). Although this type of transplant also labelled epidermis, Schwann cells and blood vessels, it cleanly excluded muscle (Supplementary Fig. 4a, b). As shown in Fig. 1b, the skin grafts generated a large swath of GFP^+ cells in the regenerated limb.

To analyse whether GFP^+ skin transplants produced skeletal muscle during regeneration, PAX7 immunofluorescence was used to identify muscle progenitors. Mid-bud-stage blastemas harbouring dermis-derived GFP^+ cells showed no overlap between GFP^+ and $PAX7^+$ cells, indicating that dermal cells did not enter the myogenic lineage (Fig. 1c, Supplementary Fig. 5 and Supplementary Table 2a). In addition, single-cell polymerase chain reaction (Supplementary Fig. 9a) of GFP^+ blastema cells showed that no dermis-derived blastema cells scored positive for *Myf5* expression, whereas 31% of control skeletal muscle-derived blastema cells expressed detectable *Myf5* (Fig. 3d).

We confirmed these results by examining fully regenerated limbs using muscle-specific-myosin heavy chain (MHCI) and PAX7 as molecular muscle markers. Although abundant GFP^+ cells intermingled with muscle tissue, no GFP^+, $MHCI^+$ muscle fibres or GFP^+, $PAX7^+$ cells were found, indicating that dermal cells do not make muscle (Fig. 1d–f, Supplementary Table 2b). We did, however, observe significant numbers of GFP^+ cells in cartilage and tendons (Fig. 1g, h and Supplementary Table 2b). Furthermore, the cells intermingling with muscle presumably represent connective-tissue fibroblasts for which there is currently no reliable marker.

The full-thickness skin transplants contained several cell types, so limited conclusions could be drawn from the above experiments. To determine whether cartilage cells truly derived from the dermis and second, if dermal cells can transdifferentiate into Schwann cells, we cleanly labelled the dermis by transplanting GFP^+ embryonic lateral plate mesoderm (which forms limb dermis, connective fibroblasts and cartilage) (see Supplementary Materials and Methods). After growing the animals to 8 cm length, limb skin (unlabelled epidermis and labelled dermis) was transplanted from the labelled animals onto GFP^- hosts and then amputated. Cartilage cells formed from these clean dermis-labelled limbs. Second, GFP^+ Schwann cells were not found in the regenerate (Supplementary Table 2c). Taken together, our dermis tracking indicates that dermis cells do not enter the myogenic or the Schwann cell lineage but do form cartilage, connective tissue and tendons.

Cartilage does not produce muscle

We also tracked the descendants of the limb skeleton. At the juvenile stages used in our experiments, the skeleton consists of cartilage. To follow limb cartilage, pieces of GFP^+ upper-arm cartilage were used

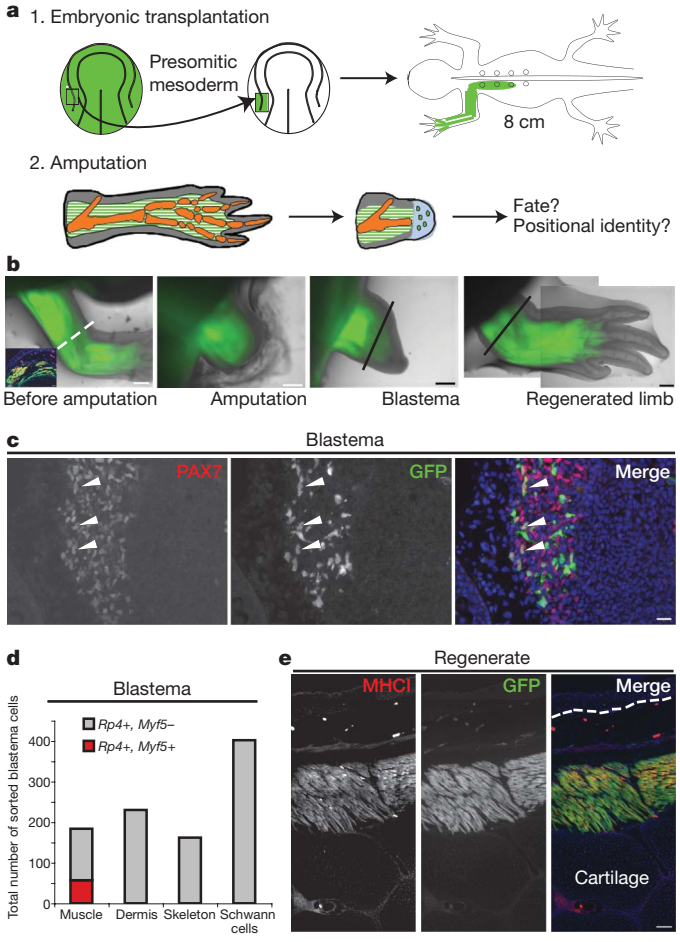

Figure 3 | Muscle does not make cartilage or epidermis. **a**, Schematic of labelling. **b**, Time course. Inset shows cross-section at dashed line (see Supplementary Fig. 4e). **c**, Section of 12-day blastema. GFP^+ cells (arrowheads) were positive for PAX7. **d**, Single-cell PCR showed that GFP^+ muscle-derived blastema cells expressed *Myf5* (see also Supplementary Fig. 9a) but GFP^+ cells from other tissues did not. RP4 acted as quality control. Numbers of cells/blastemas/animals/experiments analysed were as follows for each tissue. Skeleton: 152/8/8/4, Schwann cells: 402/6/6/6, dermis: 230/12/12/6, muscle: 184/6/6/3. **e**, Longitudinal section through regenerated limb. No GFP^+ cells were found in cartilage or epidermis (above dotted line). Scale bars: **b**, 0.5 mm; **c**, 50 μm; **e**, 100 μm.

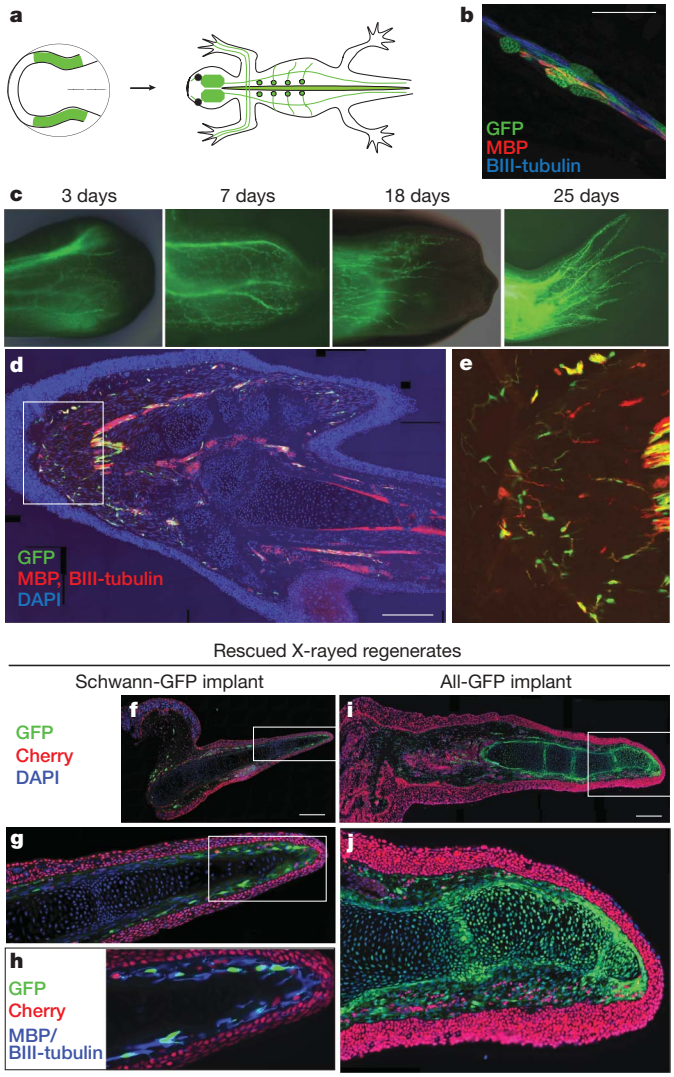

Figure 4 | Schwann cells give rise to Schwann cells and do not form cartilage even during nerve-rescue of irradiated limbs. **a**, Schematic of labelling. **b**, Confocal fluorescence image of GFP^+ Schwann cells in the hand. **c**, Time course of regeneration. Note that Schwann cells did not enter the distal tip until 25 days post amputation. **d**, Longitudinal section through a regenerated hand. GFP^+ Schwann cells were closely associated to MBP and BIII-tubulin staining. **e**, Enlarged part of **d** shown without DAPI. **f–j**, Sections of regenerating limbs that had been X-rayed and rescued by a non-irradiated nerve implant. **f–h**, A regenerate rescued by nerve with GFP-labelled Schwann cells. Cartilage was negative for both GFP and nuclear Cherry. **i, j**, A regenerate rescued by nerve tissue in which all cells expressed GFP. Cartilage cells were GFP^+, indicating that they derived from non-Schwann cells in the nerve. **g, j**, Higher magnification of the regions framed in **f** and **i** respectively. **h**, Higher magnification of the frame in **g** showing MBP and BIII-tubulin staining. Scale bars: **b**, 50 μm, **d**, **f**, **i**, 0.5 mm.

to replace a section of cartilage in GFP^- hosts before amputation (Fig. 2a, Supplementary Fig. 4c, d). GFP^+ cells contributed significantly to the blastema and then to the regenerated cartilage (Fig. 2b).

Analogously to the dermis analysis, we looked for muscle formation. No GFP^+, $PAX7^+$ or GFP^+, $Myf5^+$ cells were found in the blastema (Fig. 2c, 3d, Supplementary Table 3a), nor any GFP^+, $MHCI^+$ muscle fibres or GFP^+, $PAX7^+$ satellite cells in the regenerated limbs (Fig. 2d, Supplementary Table 3b). GFP^+ cells were observed in tendons, perichondrium and perhaps dermis (Fig. 2d). This indicates that the cells in the cartilagenous skeleton do not form myogenic cells and the vast majority contribute back to cartilage.

Muscle does not make cartilage or epidermis

Muscle was of particular interest because previous experiments indicated that muscle may produce a generalized stem cell[9,10,20,21]. We therefore transplanted GFP^+ embryonic presomitic mesoderm (Fig. 3a) to label limb muscle fibres and satellite cells (Supplementary Figs 4e and 6, Supplementary Table 4a). This method also labelled some blood vessels, as shown by autofluorescent blood cells circulating within GFP^+ vessel segments (Supplementary Fig. 6d). Amputation of the labelled limbs resulted in abundant GFP^+ cells in the regenerate (Fig. 3b–e, Supplementary Table 4b, c). Longitudinal sections representing labelling of over 25,000 nuclei in GFP^+ muscle fibres revealed no GFP^+ cells in the cartilage or epidermis (Fig. 3e, Supplementary Table 4c), indicating that muscle remains restricted primarily or exclusively to the muscle lineage.

Irradiation rescue does not increase potency

Schwann cells have also been proposed to dedifferentiate into diverse cell types during limb regeneration and such plasticity seemed plausible considering their neural crest origin[7,22,23]. To label Schwann cells we grafted GFP^+ neural fold using *white* mutant embryos as hosts and donors[24] (Fig. 4a, see Supplementary Information and the online-only Methods). The specificity of cell labelling was confirmed by the close association of the GFP signal with neuronal-specific

BIII-tubulin and glia-specific myelin basic protein (MBP) (Fig. 4b). Upon limb amputation and regeneration, surprisingly, GFP expression was clearly restricted to nerve tracts and we observed no label in cartilage or muscle (Fig. 4d, e, Supplementary Table 5a).

Our results so far found restricted cell potential during normal regeneration. To test whether cells display increased potency when forced to reconstitute other limb tissues, we examined the ability of implanted nerves to rescue irradiated limbs. To track Schwann cells versus host cells we irradiated host forelimbs transgenic for the nuclear Cherry gene. After limb amputation, we implanted nerves from the animals described above in which the Schwann cells were specifically GFP^+ (termed 'Schwann–GFP'). Longitudinal sections of the nerve-rescued samples revealed the formation of cartilage but little if any muscle. Surprisingly, the vast majority of GFP label was limited to BIII-tubulin/MBP-positive nerve tracts and the cartilage was completely negative for both transgenes (Fig. 4f–h, Supplementary Table 5b).

These results raised two alternatives; either Schwann cells were transdetermining to cartilage and the GFP transgene became silenced or the regenerated cartilage derived from an unlabelled, non-Schwann cell in the nerve. To address these possibilities we rescued nuclear Cherry-irradiated limbs with nerves from fully transgenic GFP animals ('all-GFP'). Representative sections from two of the rescued limbs revealed that all cartilage cells were GFP^+ and that no observable muscle had formed (Fig. 4i, j, Supplementary Table 5b). These results demonstrate that cartilage does not derive from Schwann cells when nerve implants rescue irradiated limbs but rather come from another cell population, presumably connective-tissue fibroblasts. Consistent with our tracking of cell potential during normal regeneration, we also saw no evidence of muscle being formed from the implanted or host tissue.

Positional identity is tissue specific

These tracking experiments have established that the blastema is a heterogeneous pool of progenitor cells from the outset of regeneration. This result has important implications for another central problem in limb regeneration—the control of positional identity along the proximal/distal limb axis. So far, experiments addressing this issue have treated the blastema as a homogeneous pool of cells[25–28]. Considering the results above, we examined whether blastema cells deriving from different tissues all harbour similar molecular and cellular features of positional identity.

We first compared cartilage and Schwann-derived blastema cells for their expression of molecular markers associated with proximo-distal identity, namely nuclear MEIS 1+2 protein and *HoxA13* messenger RNA. During limb regeneration, nuclear-localized MEIS is found in the proximal half of the upper-arm blastema (Supplementary Fig. 7a) and functions to specify upper-arm cell identity during both limb development and regeneration[29,30]. We examined whether blastema cells derived from upper-arm GFP cartilage or upper-arm GFP Schwann-cell transplants expressed nuclear-localized MEIS, and found contrasting results for the two cell types. While 95% of upper-arm-cartilage-derived blastema cells at the base of the blastema displayed nuclear-localized MEIS, no Schwann-cell-derived blastema cells displayed nuclear MEIS (Supplementary Fig. 8a–d). A portion of dermis and muscle-derived blastema cells displayed nuclear MEIS. All blastemas eventually produced a hand, so we also examined the distal-identity-associated marker *HoxA13* by single-cell PCR. *HoxA13* plays an important role in hand formation and is re-expressed in the blastema[31,32] (Supplementary Fig. 7b). 15% of upper-arm-cartilage-derived cells were positive for *HoxA13*, while so far no Schwann cells have scored positive for *HoxA13* (Supplementary Fig. 9b). This molecular data predicts that cartilage cells possess proximo-distal positional identity while Schwann cells do not.

To test the molecular prediction, we asked whether cartilage and Schwann cells behave differently in a functional assay of proximo-distal positional identity. Previous studies showed that a wrist-level blastema grafted onto an upper-arm blastema homes to the hand region during regeneration, indicating that the transplanted cells stably retain their distal identity[25,28]. To examine tissue-specific behaviours in this assay, we grafted GFP^+ fingertip cartilage into the upper arm and allowed healing before amputation. In a parallel set of limbs, we grafted upper-arm cartilage into the upper arm (Fig. 5a–c). Upon limb amputation the finger-cartilage-derived blastema cells homed to the regenerated hand (Fig. 5c, d and Supplementary Table 6), whereas control upper-arm-cartilage transplants were found all along the limb (Fig. 5b, d and Supplementary Table 6). In contrast, when we transplanted hand-derived Schwann cells into the upper arm they spread all along the proximo-distal limb axis, behaving indistinguishably from upper-arm Schwann cells (Fig. 5e, Supplementary Table 6).

The functional assays combined with the molecular results strongly indicate that cartilage cells have proximo-distal positional identity while Schwann cells are neutral and probably spread along the limb promiscuously. In general, these results indicate that the tissue origin of the blastema cell must be considered when studying positional identity.

Discussion

This work resolves many ambiguities surrounding cell plasticity during limb regeneration and points out the importance of high-resolution, genetic methods to map cell fate accurately in complex tissues *in vivo*. Our results show that limb blastema cells do not switch between embryonic germ layers and most cell types are largely restricted to their own tissue identity during limb regeneration (Supplementary Fig. 1a). Dermis was the most flexible tissue,

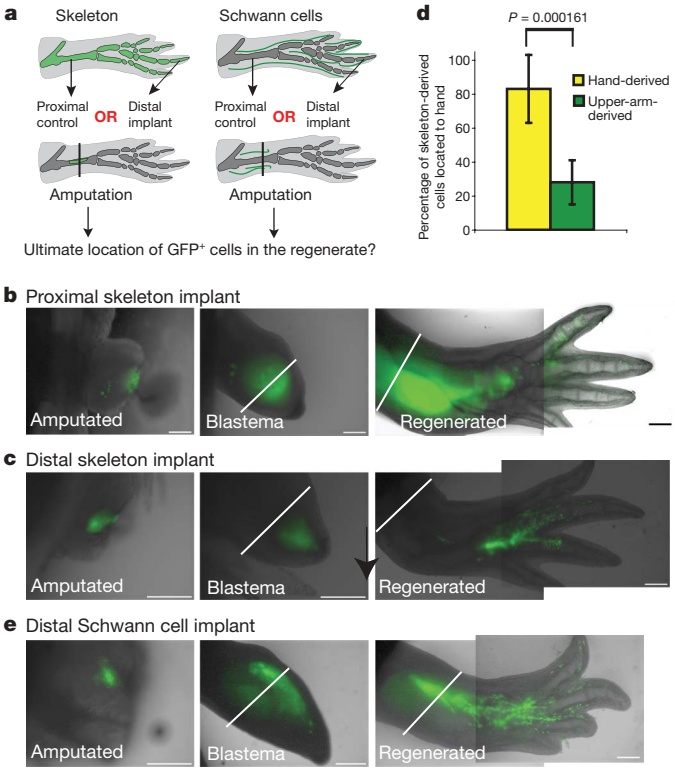

Figure 5 | Schwann cell-derived blastema cells do not possess proximo-distal positional identity but cartilage-derived cells do. **a**, Schematic to show the experimental design. **b**, **c**, **e**, Time course through regeneration of the indicated graft type. Progeny of distal skeletal cells localize distally while Schwann-cell-derived cells show no positional preference. $n = 14$ (**b**), 20 (**c**) and 15 (**e**) limbs. Scale bars: 0.5 mm. **d**, Percentage of cartilage-derived progeny originating from upper arm (six limbs) or hand transplants (seven limbs) that contribute to hand skeleton after regeneration. Error bars are standard deviations; *P* value is from Student's *t*-test (Welch; unpaired).

forming cartilage and tendons but not muscle. This attribute probably reflects the common origin of limb dermis and cartilage in the lateral plate mesoderm and suggests that dermal tissue contributes a lateral plate-like restricted progenitor in the blastema, either via a resident stem cell or reversion of a fibroblast phenotype.

Muscle and Schwann cell dedifferentiation to a multi- or pluripotent state has been an important theme in limb regeneration studies[8–10,22,33–36]. We posit that the discrepancy between our results and previous ones derives either from previous contamination of implanted cells, plasticity induced by culturing and/or labelling with invasive or leaky methods. Although we clearly demonstrate that muscle makes muscle but not cartilage or epidermis, we did not resolve here whether the regenerated muscle derives from satellite cells, dedifferentiation of muscle or both, because our current experiments labelled both muscle satellite cells and differentiated fibres. It will clearly be important to apply genetic labelling methods to resolve whether muscle dedifferentiation does indeed occur during limb regeneration.

Cell plasticity of neural cells has also been reported during tail regeneration, in which cell tracking by transient electroporation of expression plasmids led to the conclusion that spinal cord radial glia can cross lineage boundaries to form muscle and cartilage[37]. We are currently re-exploring this issue using transgenesis methods (V. Mazurov, L. Mchedlishvili and E.M.T., unpublished work)[38].

Limb regeneration studies have historically been performed on various species at different life stages, so whether the cell behaviours observed here are somehow specific for the species or the developmental stage of the animals that were used in this study is still unclear. We recapitulated a number of these experiments on sexually mature animals, so the results are unlikely to be a stage-dependent trait (data not shown). It will clearly be important to perform analogous experiments in *Notophthalmus viridescens*, in which much of the work examining muscle cell plasticity has been performed. Muscle dedifferentiation to a mononucleate state has been described in both *Notophthalmus viridescens* and *Ambystoma mexicanum*, but results showing contributions to other tissues such as cartilage has been described only in the former[9,34,35].

Importantly, this knowledge changes our common conception of the blastema from a homogeneous pool of progenitors to a group of cells that are heterogeneous from the outset. In fact, our tracking data indicate that blastema cells from the different tissues occupy distinct subregions, as summarized in Supplementary Fig. 1b. Interestingly, the dermis occupies the distal tip of the blastema and has potential to form cartilage, so a significant part of the regenerated hand skeleton derives from the dermis (Supplementary Fig. 10).

These results strikingly point to salamander blastema cells behaving, in terms of tissue-specific restrictions, like their counterparts in the mammal or like progenitors observed in the limb bud. Nonetheless, the adult salamander tissue uniquely generates these blastema cells to reconstitute an entire limb after amputation, a property that other systems do not have. It is likely that cells at the amputation plane are indeed undergoing reprogramming events that allow them to re-enter embryonic programs of tissue formation, even if they do not revert back to the earliest pluripotent state. How this is achieved in the salamander and why it does not occur in mammals remains an important question.

METHODS SUMMARY

To obtain tissue-specific GFP labelling, transgenic embryos ubiquitously expressing GFP or nuclear Cherry were used as donors for transplanting various embryonic anlagen (lateral ectoderm, neural fold, presomitic mesoderm, lateral plate mesoderm) to normal host embryos of the same stage that were then allowed to grow to a size of 8 cm. In a separate set of experiments, 8-cm-long juveniles were used as donors for transplanting full-thickness skin or cartilage to normal hosts of the same age. Limbs were amputated and descendants of fluorescently labelled tissues were followed over time and imaged using a fluorescence stereomicroscope coupled to a digital imaging system (Olympus). At different time points, limbs were processed for cryosectioning and immunofluorescence using antibodies to different cell populations (see full list of antibodies in Supplementary Information and the online-only Methods). Alternatively, blastema cell samples were dissociated by digestion with liberase (Roche), and then sorted by fluorescence-activated cell sorting (FACS) based on GFP fluorescence and DRAQ5 staining, followed by single-cell PCR (see Supplementary Information and the online-only Methods for additional information).

Full Methods and any associated references are available in the online version of the paper at www.nature.com/nature.

Received 26 February; accepted 22 May 2009.

1. Umanski, E. E. The regeneration potencies of axolotl skin studied by means of exclusion of the regeneration capacity of tissues through exposure to x-rays. *Bull. Biol. Med. Exp. USSR* **6,** 141–145 (1938).
2. Weiss, P. Unabhängigkeit der Extremitätenregeneration vom Skelett (bei *Triton cristatus*) '*Wilhelm Roux*'. *Arch. Entwicklungsmech. Organ.* **104,** 359–394 (1925).
3. Thornton, C. S. The histogenesis of the regenerating fore limb of larval Amblystoma after exarticulation of the humerus. *J. Morphol.* **62,** 219–235 (1938).
4. Namenwirth, M. The inheritance of cell differentiation during limb regeneration in the axolotl. *Dev. Biol.* **41,** 42–56 (1974).
5. Dunis, D. A. & Namenwirth, M. The role of grafted skin in the regeneration of x-irradiated axolotl limbs. *Dev. Biol.* **56,** 97–109 (1977).
6. Lheureux, E. The origin of tissues in the X-irradiated regenerating limb of the newt *Pleurodeles waltlii*. *Prog. Clin. Biol. Res.* **110,** 455–465 (1983).
7. Wallace, B. M. & Wallace, H. Participation of grafted nerves in amphibian limb regeneration. *J. Embryol. Exp. Morphol.* **29,** 559–570 (1973).
8. Echeverri, K. & Tanaka, E. M. Mechanisms of muscle dedifferentiation during regeneration. *Semin. Cell Dev. Biol.* **13,** 353–360 (2002).
9. Lo, D. C., Allen, F. & Brockes, J. P. Reversal of muscle differentiation during urodele limb regeneration. *Proc. Natl Acad. Sci. USA* **90,** 7230–7234 (1993).
10. Morrison, J. I., Loof, S., He, P. & Simon, A. Salamander limb regeneration involves the activation of a multipotent skeletal muscle satellite cell population. *J. Cell Biol.* **172,** 433–440 (2006).
11. Burns, T. C. *et al.* Thymidine analogs are transferred from prelabeled donor to host cells in the central nervous system after transplantation: a word of caution. *Stem Cells* **24,** 1121–1127 (2006).
12. Sobkow, L., Epperlein, H. H., Herklotz, S., Straube, W. L. & Tanaka, E. M. A germline GFP transgenic axolotl and its use to track cell fate: dual origin of the fin mesenchyme during development and the fate of blood cells during regeneration. *Dev. Biol.* **290,** 386–397 (2006).
13. Gargioli, C. & Slack, J. M. Cell lineage tracing during *Xenopus* tail regeneration. *Development* **131,** 2669–2679 (2004).
14. Hay, E. D. & Fischman, D. A. Origin of the blastema in regenerating limbs of the newt *Triturus viridescens*. An autoradiographic study using tritiated thymidine to follow cell proliferation and migration. *Dev. Biol.* **3,** 26–59 (1961).
15. Carlson, B. M. Morphogenetic interactions between rotated skin cuffs and underlying stump tissues in regenerating axolotl forelimbs. *Dev. Biol.* **39,** 263–285 (1974).
16. Maden, M. & Mustafa, K. The structure of 180 degrees supernumerary limbs and a hypothesis of their formation. *Dev. Biol.* **93,** 257–265 (1982).
17. Slack, M. J. Morphogenetic properties of the skin in axolotl limb regeneration. *J. Embryol. Exp. Morphol.* **58,** 265–288 (1980).
18. Muneoka, K., Fox, W. F. & Bryant, S. V. Cellular contribution from dermis and cartilage to the regenerating limb blastema in axolotls. *Dev. Biol.* **116,** 256–260 (1986).
19. Rollman-Dinsmore, C. & Bryant, S. V. The distribution of marked dermal cells from small localized implants in limb regenerates. *Dev. Biol.* **106,** 275–281 (1984).
20. Asakura, A., Komaki, M. & Rudnicki, M. Muscle satellite cells are multipotential stem cells that exhibit myogenic, osteogenic, and adipogenic differentiation. *Differentiation* **68,** 245–253 (2001).
21. Wada, M. R., Inagawa-Ogashiwa, M., Shimizu, S., Yasumoto, S. & Hashimoto, N. Generation of different fates from multipotent muscle stem cells. *Development* **129,** 2987–2995 (2002).
22. Wallace, H. The components of regrowing nerves which support the regeneration of irradiated salamander limbs. *J. Embryol. Exp. Morphol.* **28,** 419–435 (1972).
23. Horstadius, S. & Sellmann, S. Experimentelle Untersuchungen uber die Determination des knorpeligen Kopfskelettesbei Urodelen. *Nova Acta Regiae Soc. Sci. Ups. Ser.* **13,** 1–170 (1946).
24. Epperlein, H., Meulemans, D., Bronner-Fraser, M., Steinbeisser, H. & Selleck, M. A. Analysis of cranial neural crest migratory pathways in axolotl using cell markers and transplantation. *Development* **127,** 2751–2761 (2000).
25. Crawford, K. & Stocum, D. L. Retinoic acid coordinately proximalizes regenerate pattern and blastema differential affinity in axolotl limbs. *Development* **102,** 687–698 (1988).
26. Iten, L. E. & Bryant, S. V. The interaction between the blastema and stump in the establishment of the anterior–posterior and proximal–distal organization of the limb regenerate. *Dev. Biol.* **44,** 119–147 (1975).
27. Nardi, J. B. & Stocum, D. L. Surface properties of regenerating limb cells: evidence for gradation along the proximodistal axis. *Differentiation* **25,** 27–31 (1983).
28. Echeverri, K. & Tanaka, E. M. Proximodistal patterning during limb regeneration. *Dev. Biol.* **279,** 391–401 (2005).
29. Mercader, N. *et al.* Conserved regulation of proximodistal limb axis development by Meis1/Hth. *Nature* **402,** 425–429 (1999).

30. Mercader, N., Tanaka, E. M. & Torres, M. Proximodistal identity during vertebrate limb regeneration is regulated by Meis homeodomain proteins. *Development* **132,** 4131–4142 (2005).
31. Gardiner, D. M., Blumberg, B., Komine, Y. & Bryant, S. V. Regulation of HoxA expression in developing and regenerating axolotl limbs. *Development* **121,** 1731–1741 (1995).
32. Fromental-Ramain, C. *et al.* Hoxa-13 and Hoxd-13 play a crucial role in the patterning of the limb autopod. *Development* **122,** 2997–3011 (1996).
33. Kumar, A., Velloso, C. P., Imokawa, Y. & Brockes, J. P. Plasticity of retrovirus-labelled myotubes in the newt limb regeneration blastema. *Dev. Biol.* **218,** 125–136 (2000).
34. Kumar, A., Velloso, C. P., Imokawa, Y. & Brockes, J. P. The regenerative plasticity of isolated urodele myofibers and its dependence on MSX1. *PLoS Biol.* **2,** E218 (2004).
35. Echeverri, K., Clarke, J. D. & Tanaka, E. M. *In vivo* imaging indicates muscle fiber dedifferentiation is a major contributor to the regenerating tail blastema. *Dev. Biol.* **236,** 151–164 (2001).
36. Tanaka, E. M. Regeneration: if they can do it, why can't we? *Cell* **113,** 559–562 (2003).
37. Echeverri, K. & Tanaka, E. M. Ectoderm to mesoderm lineage switching during axolotl tail regeneration. *Science* **298,** 1993–1996 (2002).
38. Mchedlishvili, L., Epperlein, H. H., Telzerow, A. & Tanaka, E. M. A clonal analysis of neural progenitors during axolotl spinal cord regeneration reveals evidence for both spatially restricted and multipotent progenitors. *Development* **134,** 2083–2093 (2007).

Supplementary Information is linked to the online version of the paper at www.nature.com/nature.

Acknowledgements This work was supported by grants from the Volkswagen Foundation I/78 766; DFG SFB655, SPP1109, SPP 1356, the BMBF Biofutures program, funds from the Max Planck Institute, and the Center of Regenerative Therapies, Dresden. D.K. was a fellow of the Alexander von Humboldt Foundation. We are grateful to K. Agata, H. Tarui, T. Hayashi and M. Saitou for advice on the single-cell PCR technique. We thank I. Nüsslein for assistance on FACS analysis and A. Merseburg for assistance on the nerve rescue experiments. We thank H. Andreas, T. Richter and M. Schuez for technical assistance. We are grateful to L. Rohde, C. Antos, G. Weidinger and A. Tóth for comments on the manuscript.

Author Contributions M.K., D.K. and E.M.T. designed the experiments. M.K., D.K., E.N. and H.H.E. performed embryonic grafting and specificity assessment. M.K. imaged and performed the histological analysis of regenerating limbs, cell counting and single-cell PCR on all experiments. D.K. performed all work related to Schwann cells, with M.M.'s advice. S.K. generated the nucCherry transgenic animals. E.M.T. advised on experiments, examined samples and evaluated data. M.K., D.K. and E.M.T. wrote the manuscript.

Author Information Reprints and permissions information is available at www.nature.com/reprints. Correspondence and requests for materials should be addressed to E.M.T. (elly.tanaka@crt-dresden.de).

METHODS

Axolotl care. *Ambystoma mexicanum* individuals (axolotls) were bred in our facility, where they were kept at 18 °C in Dresden tap water and fed daily with artemia or fish pellets. For all surgery, animals were anaesthetized in 0.01% ethyl-*p*-aminobenzoate (Sigma). The experiments described here were performed on 8-cm-long juvenile axolotls.

Transgenesis. The generation of transgenic animals ubiquitously expressing GFP under the control of the CAGGS promotor has been described before[39]. Following the same protocol, transgenic animals expressing nuclear Cherry under the control of the CAGGS promotor were generated.

Fluorescent cells were imaged live using a 25× or 40× plan-neofluar objective on a Zeiss Axiovert 200 system with a Spot digital camera, controlled by MetaMorph image acquisition software.

Embryonic transplantation. We labelled the respective tissues by transplantation of GFP^+ embryonic or mature tissue to normal hosts. After the embryos had developed into juveniles (~8 cm snout to tail), limbs were amputated through regions containing fluorescent cells. Such grafts ultimately labelled a significant portion of a given limb tissue so that when we observed no contribution of labelled cells to another tissue layer after regeneration, the result securely reflected a tissue-specific restriction. This level of numerical significance would not have been achievable by tracing techniques, in which one cell is labelled per animal to determine cell lineage. A similar approach has been used successfully to analyse *Xenopus* tail regeneration[40].

An important requirement of the donors is the stability of transgene expression. We used the ubiquitous CAGGS promoter to drive GFP, resulting in stable expression except in some blood cells[39,41]. No evidence of chimaeric expression in regenerating limbs to indicate silencing was observed (Supplementary Fig. 2 and Supplementary Table 1).

To specifically label epidermis, Schwann cells or muscle tissue in the axolotl limb, we performed transplantation of the respective embryonic anlage to host embryos. Briefly, normal and transgenic embryos were allowed to reach late gastrulae (stage 13) before being dejellied. For the surgical procedure, stage 14–18 embryos were transferred to agar dishes containing 1× Steinberg's saline with antibiotics. Prior to operations, they were kept for 1 h at 4 °C. Then the vitelline membrane was removed.

Epidermis: an epidermal sheet of about 1 mm^2 was excised from the limb fields of stage 18 embryos (ventro-lateral region at somite level 3–4). At this stage, the epidermal layer can be removed without contaminating underlying mesodermal tissue. From GFP^+ transgenic animals, an epidermal piece of the same size was removed and transplanted onto the operated site of the host embryo. Embryos that received a fluorescent epidermal graft were grown to the size of 2 cm larvae before experimental analyses were performed (Supplementary Fig. 3a). The transplanted cells were restricted to the epidermal layer as assessed by Fibronectin localization, which demarcates the epidermal basement membrane (Supplementary Fig. 3b). In the regenerated limb, GFP^+ cells were still restricted to the epidermal layer, confirming the previous findings that epidermis does not contribute to other limb tissues (Supplementary Fig. 3c).

Dermis: in stage 17–20 embryos the epidermal layer was lifted up and the underlying lateral plate mesoderm was removed from the host. Equivalent pieces of lateral plate mesoderm were taken from the GFP^+ donors and placed into the hosts, after which the epidermal flap was closed over the transplanted cells.

Muscle: at stage 14–15 the neural fold of host embryos at somite level 3–5 was detached using tungsten needles and pieces of the underlying presomitic mesoderm were removed from the region where progenitors of the limb muscle tissue normally reside. Transgenic embryos were opened in the same way, and fluorescent grafts of the respective tissue layer were transferred to the host. After the surgery, the epidermis was folded back. We observed labelling of muscle fibres and satellite cells after the embryos had developed into juveniles (Supplementary Figs 4e and 6a). We also observed labelling in some blood vessels, presumably owing to endothelial precursors contaminating the original graft.

Schwann cells: neural folds of stage 14–16 *white* mutant host embryos were removed all along the antero-posterior axis and replaced by GFP^+ fluorescent neural folds derived from transgenic, *white* mutant stage 14–16 donor embryos. Several neural-crest-derived cell types were fluorescently labelled in adults that received fluorescent neural fold transplants during their embryogenesis. However, melanophores and Schwann cells are the only neural-crest-derived cell types present in the limb. This operation produced specific labelling of Schwann cells in the limb because in *white* embryos melanophores do not migrate away from the neural tube region, leaving the limb free of melanophores. Axolotls whose limbs harboured fluorescent Schwann cells were either directly used for experiments, or pieces of tissue containing GFP^+ Schwann cells were transplanted and analysed in normal hosts.

Axolotl surgery. Surgeries to specifically label animals for skin or skeleton were performed on 8-cm-long (snout to tail) juveniles. As donors, we used GFP-transgenic animals.

Full-thickness skin: squares of ~1 mm × 1 mm were excised from the dorsal upper arm skin of GFP^+ transgenic donors. After removal of contaminating pieces of muscle and large nerves, they were grafted to the dorsal site of a normal host where a large piece of skin had been removed before surgery. After an integration period of 2 weeks, limbs were amputated through the grafts.

Skeleton: upper arm and hand skeletal elements were removed from GFP^+ transgenic donors and incubated for 30–60 min in 80% PBS containing 30 U ml^{-1} papain (Sigma) and 10 U ml^{-1} DNase IV (Roche) to clear them of contaminating tissues such as muscle and nerves. Fluorescent tissues were then implanted into the upper arms of normal hosts from which a large piece of skeletal tissue had been removed before surgery. After a healing period of 2 weeks, limbs were amputated through the grafts.

X-ray irradiation and nerve implantation. Experiments were performed on 6–8-cm-long animals. The limbs of narcotized animals were irradiated in an X-ray machine (YXLON International, Maxishot, 1000426 B) at 200 kV and 20 mA for 3.3 min, which at a 16 cm distance from the source gave a dose of 20 Gy. The other body parts were shielded by 3-mm-thick lead plates, which transmitted less than 5% of the incident dose.

Nerves from non-irradiated donors containing either GFP-labelled Schwann cells or all cells GFP^+ were explanted in 80% PBS, cleaned of contaminating sticking cells, implanted into the irradiated lower arms through a small incision in the skin, and two days later the limbs were amputated through the implant. Within 22–40 weeks (a period much longer than is sufficient to allow the regeneration of unirradiated control limbs) a significant number of the X-rayed limbs that received a nerve implant produced limbs that were not completely patterned. Five of 17 irradiated limbs were rescued by Schwann–GFP nerve, and five of 16 irradiated limbs were rescued by the 'all-GFP' nerve implants. The unrescued controls continuously lost tissue up to the shoulder.

Antibody staining on axolotl limb cryosections. Axolotl limbs were fixed in fresh 4% paraformaldehyde overnight at 4 °C, washed in PBS, incubated in 30% sucrose overnight and frozen in Tissue-Tek (O.C.T. compound, Sakura) or in 7.5% gelatin (Merck). Cross- and longitudinal- limb sections (14–20-μm-thick) were washed in TBS/0.3% Tween and blocked for one hour in 20% goat serum, followed by an overnight incubation with anti-Pax7 mAB (Developmental Studies Hybridoma Bank), anti-MEIS pAB (Upstate Cell Signalling solution), anti-MBP pAB (Gene Tex Industries) and anti-BIII-tubulin mAB (R&D Systems). After several washes in TBS/Tween, a Cy5-labelled anti-mouse secondary antibody (Dianova) was used at 1:200 dilution in combination with anti-PAX7, anti-MEIS and anti-BIII-tubulin primary antibodies, while a Cy3- or Cy5-labelled anti-rat secondary antibody was used at a 1:100 dilution in combination with the anti-MBP primary antibody. To visualize $MHCI^+$ muscle fibres, we used the monoclonal antibody 4A1025 (the kind gift of S. Hughes), which was directly coupled to rhodamine-NHS (Molecular Probes). Nuclear stainings were performed using DAPI or 1 μg ml^{-1} of Hoechst in TBS/Tween20.

Images were taken on an Olympus BX61 microscope using a digital camera (Diagnostic Instruments Inc.) under the control of the Spot Advanced program. Mosaic images in Supplementary Figs 5 and 7 were stitched using the Adobe Photoshop CS3 program. Mosaic images in Supplementary Fig 4d–j were taken on a Zeiss Observer Z1 and stitched using the AxioVision program. Confocal images were acquired on a Zeiss LSM 510 microscope.

Cell dissociation and FACS. In each experiment, two limb blastemas were manually dissected in 2 ml liberase based dissociation solution (100 U ml^{-1} DNase IV, 0.35 mg ml^{-1} liberase blendzyme both Roche, in 80% PBS), until a single-cell suspension was visible (depending on the tissue, 10–60 min). The cell suspension was transferred into a new tube incubated with 5 μM DRAQ5 (Axxora). Cells were then passed through a 22-μm filter and analysed by FACS. Single events of maximum GFP intensity, which were verified to be GFP^+ transgenic cells, were gated and sorted into reverse transcription buffer.

Single-cell PCR. Single-cell PCR was performed as described[42] with the following modifications.

Reverse transcription: cells were sorted into a 96-well plate in which each well contained 5 μl reverse transcription buffer. The plate was centrifuged and incubated for 1 min at 65 °C and 3 min at 22 °C. 2.6 μl RNase-free water and 0.4 μl SSII reverse transcriptase (Invitrogen) were then added to each well so that the reverse transcription buffer reached a final volume of 8 μl containing 50 mM Tris-Cl pH 8.3, 75 mM KCl, 0.1 ng μl^{-1} reverse transcription primer (sequence: TGG ACT AAC TAT GAA TTC TTT TTT TTT TTT TTT TTT TTT V), 2 μM dNTPs, 0.5% NP40 (Sigma), 0.08 μl RNAguard (GE Healthcare) and 0.27 μl Prime RNase inhibitor (VWR). For reverse transcription, the plate was incubated at 42 °C for 15 min and 70 °C for 10 min.

Poly A tailing: to each reaction well, 8 μl polyadenylation solution was added to reach a final concentration of 100 mM of potassium cacodylate (Roche), 2 mM of $CoCl_2$ (Roche), 0.2 mM of DTT, 100 μM of dATP and 0.2 μl terminal transferase (Roche) were added to reach a final volume of 16 μl. The plate was incubated at 37 °C for 15 min and at 65 °C for 10 min.

PCR: the reaction volume was increased to 50 μl for PCR amplification to reach a final concentration of 1× reaction buffer, 1 mM dNTPs, 0.07 μg μl^{-1} PCR primer (sequence: CAT GTC GTC CAG GCC GCT CTG GGA CAA AAT ATG AAT TC TTT TTT TTT TTT TTT TTT TTT TTT) and 0.1 U μl^{-1} TAQ polymerase (MPI-CBG protein expression facility). After one complete run (1 cycle of 37 °C for 5 min and 72 °C for 20 min; 25 cycles of 94 °C for 1 min, 42 °C for 2 min and 72 °C for 6 min plus 10 s extension/cycle), fresh TAQ polymerase was supplied along with buffer, dNTPs and PCR primer to a final volume of 60 μl and maintaining the final concentrations of each component. After the addition of the fresh components, the amplification reaction was repeated. After the completion of the second run, we normally generated a total amount of 8–10 mg complementary DNA, which was analysed subsequently in a quantitative PCR using gene-specific primers.

Real time PCR on cDNA generated by single-cell PCR. The cDNAs were diluted 1:300 and used as a template to perform quantitative PCR. Reactions were performed in a total volume of 10 μl using the SYBR Green kit (Stratagene) following the instructions given by the manufacturer. We used the recommended final primer concentration of 300 nm. Sequences of gene-specific primers were designed based on the published sequences obtained from our cDNA library[43].

The primer sequences were TGA AGA ACT TGA GGG TCA TGG forward and CTT GGC GTC TGC AGA TTT TTT reverse (*Rp4*), GGG CAC ACT AAA AAG GTT AAA forward and GCA GGG TTT ACG ACA ATG TAC reverse (*HoxA13*), and AGC AGA TTC CTG CGA TGT TT forward and GCA CCA CAT GAC AAA ACA CA reverse (*Myf5*).

Statistical analyses. Localization of cells to lower arm versus hand skeleton were analysed using the Student's *t*-test for unpaired samples (Welch modification). *P* values were determined using the Matlab software.

39. Sobkow, L., Epperlein, H. H., Herklotz, S., Straube, W. L. & Tanaka, E. M. A germline GFP transgenic axolotl and its use to track cell fate: dual origin of the fin mesenchyme during development and the fate of blood cells during regeneration. *Dev. Biol.* **290,** 386–397 (2006).
40. Gargioli, C. & Slack, J. M. Cell lineage tracing during *Xenopus* tail regeneration. *Development* **131,** 2669–2679 (2004).
41. Okabe, M., Ikawa, M., Kominami, K., Nakanishi, T. & Nishimune, Y. 'Green mice' as a source of ubiquitous green cells. *FEBS Lett.* **407,** 313–319 (1997).
42. Brady, G. & Iscove, N. N. Construction of cDNA libraries from single cells. *Methods Enzymol.* **225,** 611–623 (1993).
43. Habermann, B. *et al.* An *Ambystoma mexicanum* EST sequencing project: analysis of 17,352 expressed sequence tags from embryonic and regenerating blastema cDNA libraries. *Genome Biol.* **5,** R67,–1–19 (2004).